A G3BP1-interacting lncRNA promotes ferroptosis and apoptosis in cancer via nuclear sequestration of p53

Chao Mao [1,2,*], Xiang Wang [3,*], Yating Liu [1,2], Min Wang [1,2], Bin Yan [1,2], Yiqun Jiang [1,2,3], Ying Shi [1,2], Yi Shen [4], Xiaoli Liu [1,2], Weiwei Lai [1,2], Rui Yang [1,2], Desheng Xiao [5], Yan Cheng [6], Shuang Liu [7], Hu Zhou [8], Ya Cao [1,2], Weishi Yu [9], Kathrin Muegge[10], Herbert Yu [4], Yongguang Tao [1,2,3,+]

1 Key Laboratory of Carcinogenesis and Cancer Invasion, Ministry of Education, Xiangya Hospital, Central South University, Hunan, 410078 China

2 Key Laboratory of Carcinogenesis，Ministry of Health, Cancer Research Institute, Central South University, Changsha, Hunan, 410078 China

3 Department of Thoracic Surgery, Second Xiangya Hospital, Central South University, Changsha, China

4 Cancer Epidemiology Program, University of Hawaii Cancer Center, Honolulu, Hawaii, USA

5 Department of Pathology, Xiangya Hospital, Central South University, Changsha, Hunan, 410008 China

6 Department of Pharmacology, School of Pharmaceutical Sciences, Central South University, Changsha, Hunan 410078 China

7 Center for Medicine Research, Xiangya Hospital, Central South University, Changsha, Hunan, 410008 China

8 Shanghai Institute of Material Medica, Chinese Academy of Sciences (CAS), 555 Zu Chongzhi Road, Zhangjiang Hi-Tech Park, Shanghai, 201203, China

9 Cipher Gene (Beijing) Co., Ltd, Beijing 100089, China

10 Mouse Cancer Genetics Program, National Cancer Institute, Basic Science Program, Leidos Biomedical Research, Inc., Frederick National Laboratory for Cancer Research, Frederick, Maryland 21702, USA

* equal contribution;

[+] Corresponding author and lead contact. Y.T. Email: taoyong@csu.edu.cn; Tel. +(86) 731-84805448; Fax. +(86) 731-84470589.

Supplementary Material and Methods

Western blot analysis and Co- Immunoprecipitation (Co-IP) assay

Details of the cell proliferation assay have been described previously (1). Cells were harvested, washed twice with ice-cold phosphate-buffered saline (PBS), lysed in RIPA buffer and centrifuged at 15,000 × g for 10 min after sonication. The supernatants were collected as whole-cell lysates. A quantity of 50 µg of total protein was used for Western blot analysis. For immunoprecipitation experiments, cells were plated overnight in 100 mm^2 dishes (1.5×10^6/dish). One mg of protein was mixed with 40 µl of Protein A-Sepharose beads (Sigma) in the immunoprecipitation assay buffer (1× PBS, 0.5% Nonidet P-40, 0.5% sodium deoxycholate and 0.1% SDS), incubated at 4°C for 2 h with gentle agitation and centrifuged for 10 min at 2000 rpm for preclearing. The recovered supernatant was incubated with 10 µl of anti-Flag M2 agarose (Sigma) in the presence of 1× protease inhibitors at 4°C overnight with mild shaking. The M2 agarose-precipitated protein complex was recovered by a brief centrifugation followed by three washes with the immunoprecipitation assay buffer. The harvested beads were re-suspended in 30 µl of 2× SDS PAGE sample buffer and boiled for 5 min to release the bound protein. A 20 µg aliquot of cell lysate was used as an input control. The samples were analyzed by Western blot and the antibodies used are indicated.

The following antibodies were used: G3BP (Abcam, ab181149), G3BP1 (Santa Cruz Biotechnology cat# sc-81940), G3BP2 (Abcam, ab86135), p53 (Santa Cruz Biotechnology cat# sc-126), p21 (Cell Signaling Technology cat# 2947), MDM2 (Santa Cruz Biotechnology cat# sc-813), CDK1/2 (Santa Cruz Biotechnology cat# sc-53219), CDK4 (Santa Cruz Biotechnology cat# sc-260), Cyclin B1 (Santa Cruz Biotechnology cat# sc-7393), Cyclin D1 (Santa Cruz Biotechnology cat# sc-20044),

Caspase-3 (Cell Signaling Technology cat# 14220), Caspase-8 (Cell Signaling Technology cat# 9746), Caspase-9 (Cell Signaling Technology cat# 9502), Histone H3 (Cell Signaling Technology cat# 9715), LSH (Santa Cruz Biotechnology cat# sc-46665), CHD4 (Sigma Aldrich cat# SAB4500202), Keratin 17/19 (Cell Signaling Technology cat# 3984).

Quantitative real-time PCR and RNA sequencing

Cells were harvested with Trizol (Invitrogen). cDNA was synthesized with SuperScript III (Invitrogen) according to the manufacturer's protocol. Real-time PCR analysis was performed using the Applied Biosystems 7500 Real-Time PCR System, according to the manufacturer's instructions. The reactions were performed in triplicate for three independent experiments: the results were normalized to β-actin. The primer sequences used can be found in the Supplementary Table S5. The mean± SD of three independent experiments is shown.

For RNA sequencing, the total RNA samples were first treated with DNase I to degrade any possible DNA contamination. Then, the mRNA was enriched by using the oligo(dT) magnetic beads. The mRNA was then mixed with the fragmentation buffer and broken into short fragments. Then the first strand of cDNA was synthesized by using random hexamer-primer. Buffer, dNTPs, RNase H and DNA polymerase I were added to synthesize the second strand. The double strand cDNA was purified with magnetic beads. End reparation and 3'-end single nucleotide A (adenine) addition was then performed. Finally, sequencing adaptors were ligated to the fragments. The fragments were enriched by PCR amplification. During the QC step, the Agilent 2100 Bioanaylzer and ABI StepOnePlus Real-Time PCR System were used to qualify and quantify of the sample library. The library products were then deemed ready for sequencing via Illumina HiSeqTM 2000. The whole RNA-

sequencing process and data analysis was conducted by BGI Tech, Shenzhen, China.

Chromatin immunoprecipitation (ChIP) assays

ChIP assays were essentially performed as previously described (1) with slight modifications: 5×10^6 cells were fixed with formaldehyde (1% final volume concentration, Sigma) for 10 min at room temperature. Fixation was stopped with the addition of 1/10 volume 1.25 M glycine and the samples were incubated for 5 min at room temperature. The sonication step was performed in a Qsonica sonicator (5 min, 20 s on, 20 s off), and 200 μg of the protein-chromatin complex was used in each immunoprecipitation. Antibody-protein complexes were captured with preblocked dynabeads protein G (Invitrogen). ChIP DNA was analyzed by qPCR with SYBR Green (Biorad) on an ABI-7500 (Applied Biosystems) using the primers specified in Supplemental Table S6. The antibodies used are as followed: LSH (Santa Cruz), H3K27Me3(Active motif), H3K4Me3(Active motif), Cfp1 (Sigma), p53 (Santa Cruz) and normal mouse IgG (12-371, Millipore).

Cell proliferation, migration, invasion, and colony formation assays.

Details of the cell proliferation assay have been described previously (1). For the plate-colony formation assay, cells (2×10^3/mL/well) were seeded into 6-well plates and cultured in RPMI-1640 medium supplemented with 10% FBS. Colonies were fixed with methanol and stained with Crystal Violet, then scored using a microscope and ImageJ software (1.47V, NIH, USA).

The migration assay has been described previously (2). Cells (5×10^5) were seeded onto the upper chamber in 200 μL of serum-free medium; the lower compartment was filled with 0.6 ml of DMEM media supplemented with 10% of FBS. After a 24 hour incubation, migrated cells on the lower surface of the filter were fixed

and stained using propidium iodide. Cells on the upper side were removed using a rubber scraper. Fluorescent images were obtained. The reported data represents counts of migrated cells. Experiments were performed in triplicate.

For the plate-colony formation assay, cells (2×10^3/ml/well) were seeded into 6-well plates and cultured in RPMI-1640 medium supplemented with 10% FBS. Colonies were fixed with methanol, stained with Crystal Violet and scored using a microscope and ImageJ software (1.47V, NIH, USA).

Luciferase assay

To test the activity of the p53 pathway, we used a p53-responsive luciferase construct obtained from Dr. Zhi-Min Yuan (Harvard University). Using the described protocol, levels of luciferase activity were normalized to the expression levels of a non-responsive construct encoding Renilla.

Measurement of total ROS, Lipid ROS and Iron

Details of the procedures have been described previously (3,4). The detailed RNA seq procedure is listed into the supplementary Material and Methods.

For total ROS, cells were treated as indicated and trypsinized and resuspended in medium plus 10% FBS, then 4μM of Dihydroethidium (DHE, Sigma, Cat.# 37291) was added and samples were incubated for 15 min at 37°C, 5% CO_2 and protected from light. Excess DHE was removed by washing the cells twice with pre-warmed PBS. DHE was oxidized to highly red fluorescence ethidium which is proportional to ROS generation and was analyzed using a flow cytometer (Fortessa, BD Biosciences). More than 10 000 cells were analyzed per condition.

For Lipid ROS, cells were treated as indicated, and then typsinezed and resuspended in medium plus 10% FBS. Then, 10μM of C11-BODIPY (Thermo Fisher,

Cat# D3861) was added and samples were incubated for 30 min at 37°C, 5% CO_2 and protected from light. Excess C11-BODIPY was removed by washing the cells twice with PBS. Oxidation of the polyunsaturated butadienyl portion of the dye results in a shift of the fluorescence emission peak from 590 nm to 510 nm in a manner proportional to lipid ROS generation. This shift was analyzed using a flow cytometer.

For the Iron assay, we used the Iron Assay Kit(Sigma Aldrich) to measure the Fe^{2+} or total iron in each cell line. 2×10^6 of cells were rapidly homogenized in 4–10 volumes of Iron Assay buffer. Samples were centrifuged at 13,000 g for 10 minutes at 4℃ to remove insoluble material. To measure ferrous iron, 5μL of iron assay buffer was added to each well. To measure ferric iron, two sets of wells were set up. Then, 5μL of assay buffer was added to the samples in one set of wells and 5μL of Iron Reducer was added to the other set of wells. To measure total iron, add 5μL of Iron Reducer to each of the sample wells to reduce Fe^{3+} to Fe^{2+}. Samples were mixed well using a horizontal shaker or by pipetting, and the reactions were incubated for 30 minutes at room temperature, protected from light. Then, 100 μL of Iron Probe was added to each well containing standard or test samples. Samples were mixed well using a horizontal shaker or by pipetting, and the reactions were incubated for 60 minutes at room temperature, protected from light. Finally, the absorbance was measured at 593 nm (A_{593}).

Immunohistochemistry (IHC) analysis

Lung and related diseases biopsies were validated and obtained from the Department of Pathology in Xiangya Hospital. IHC analysis of paraffin sections from lung cancer tissues was described previously (2). The sections were incubated with antibodies as indicated. The images were surveyed and captured using a CX41 microscope (OLYMPUS, Tokyo, Japan) with the Microscope Digital Camera System DP-72 (OLYMPUS, Tokyo, Japan) and differentially quantified by two pathologists from the Xiangya Hospital, Changsha, China.

The determination results were obtained using semi-quantitative classification according to 10 or more visual fields (×200). The slides were first scored as 0 (negative), 1 (buff), 2 (pale brown), or 3 (tan). Positive expression of Cfp1 was scored as 0 (negative), 1+ (<10% of positively staining tumor cells), 2+ (11-50% of positively-staining tumor cells), 3+ (50-75% of positively staining tumor cells), and 4+ (>75% of positively staining tumor cells). These two scores were multiplied together to get the determination result.

Table S1 Plasmid construction

Name	Sequence	Product size(bp)
G3BP1-1-466-Flag	F: CGGAATTCATGGTGATGGAGAAGCCTAGTC R: CGGGATCCTTACTTATCGTCGTCATCCTTGTAATCCTGCCGTGGCGCAAGCCCCCTT	1441
G3BP1-1-173-Flag	F: CGGAATTCATGGTGATGGAGAAGCCTAGTC R: CGGGATCCTTACTTATCGTCGTCATCCTTGTAATCGAAAGTTCCAGAATCATCAGGTAC	562
G3BP1-174-466-Flag	F: CGGAATTCATGTATGATCAGGCAGTTGTCAGTAATG R: CGGGATCCTTACTTATCGTCGTCATCCTTGTAATCCTGCCGTGGCGCAAGCCCCCTT	925
G3BP1-136-336-Flag	F: CGGAATTCATGGAGGTCTTTGGTGGGTTTGTCACTG R: CGGGATCCTTACTTATCGTCGTCATCCTTGTAATCGTGTCTCACCATTCTTCGGGGTTC	649

Table S2 RNA-pull down

Name	Sequence	Product size(bp)
P53RRA -T7-1-871	F: TAATACGACTCACTATAGGGATGCGAGGCTGGGGCCGGTTGCCTA R: TGTGTTGTGTTGTCTTCCTCTC	891
P53RRA -T7-1-1770	F: TAATACGACTCACTATAGGGATGCGAGGCTGGGGCCGGTTGCCTA R: TGGAAATTGAAGAATGAGTAGAATC	1790
P53RRA -T7-1-2340	F: TAATACGACTCACTATAGGGATGCGAGGCTGGGGCCGGTTGCCTA R: CATTCCCAAGGATAATGCTATATTGTCC	2360
P53RRA 2-T7-1-2933	F: TAATACGACTCACTATAGGGATGCGAGGCTGGGGCCGGTTGCCTA R: ACTGACAGGAAAACATTTTAATTCAAACC	2953
P53RRA -T7-872-2933	F: TAATACGACTCACTATAGGGGGAGGGGATAAGTACCTCTGGACA R: ACTGACAGGAAAACATTTTAATTCAAACC	2081
P53RRA -T7-1771-2933	F: TAATACGACTCACTATAGGGGCTTCTCCTTGGAGCCTTCCCAGAT R: ACTGACAGGAAAACATTTTAATTCAAACC	1182
P53RRA -T7-2341-2933	F: TAATACGACTCACTATAGGGATTTCATATTGTTGAATAAATAGG R: ACTGACAGGAAAACATTTTAATTCAAACC	612
Antisense-LINC00472	F: TAATACGACTCACTATAGGGACTGACAGGAAAACATTTTAATTCAAACC R: ATGCGAGGCTGGGGCCGGTTGCCTA	2953

Table S3 RT-PCR primers.

Name	Full Name	Gene ID	Sequence	Product size(bp)
P53RRA	long intergenic non-protein coding RNA 472	79940	F: GGTGACTTTCTCGACTCGTCGT R: GATGATGCCAACATGTCTGGTGC	176
ATG5	autophagy related 5	9474	F: GCAGATGGACAGTTGCACACAC R: GAGGTGTTTCCAACATTGGCTCA	130
BATF3	basic leucine zipper ATF-like transcription factor 3	55509	F: ACCGAGTTGCTGCTCAGAGAAG R: AGGTGCTTCAGCTCCTCTGTCA	139
CARS	cysteinyl-tRNA synthetase	833	F: CTGGACTACTCCAGCAACACCA R: GACCAGTGATGTCAACAGGAGC	112
CDH17	cadherin 17	1015	F: GGCAATGTGACTGCCAAGGATC R: GCTTCTCTGTCCAATGGAGCCA	131
CS	citrate synthase	1431	F: CACAGGGTATCAGCCGAACCAA R: CCAATACCGCTGCCTTCTCTGT	127
CXCL1	C-X-C motif chemokine ligand 1	2919	F: AGCTTGCCTCAATCCTGCATCC R: TCCTTCAGGAACAGCCACCAGT	119
EGF	epidermal growth factor	1950	F: TGCGATGCCAAGCAGTCTGTGA R: GCATAGCCCAATCTGAGAACCAC	139
EGR2	early growth response 2	1959	F: CCTTTGACCAGATGAACGGAGTG R: GAAGGTCTGGTTTCTAGGTGCAG	131
FBLN7	fibulin 7	129804	F: AGCGGCAATGTGAGCTACGTGA R: CTTCAGGTTGGAAGGCAGAGAG	135
GPR162	G protein-coupled receptor 162	27239	F: CTCCTTCATCTGGTCCTGCGAG R: TGGCTCCGTTAGCATCAAAGCG	161
HNRNPC	heterogeneous nuclear ribonucleoprotein C	3183	F: TGGGCTGCTCTGTTCATAAGGG R: CTCGGTTCACTTTTGGCTCTGC	147
MYC	v-myc avian myelocytomatosis viral oncogene homolog	4609	F: CCTGGTGCTCCATGAGGAGAC R: CAGACTCTGACCTTTTGCCAGG	128
RIMBP3C	RIMS binding protein 3C	150221	F: CCAACTTCGTGGAGCAGATTCC R: GCTGTCTTCCTCCAGAGCTTCA	119
SLC1A5	solute carrier family 1 member 5	6510	F: TCCTCTTCACCCGCAAAAACCC R: CCACGCCATTATTCTCCTCCAC	135
SLC2A14	solute carrier family 2 member 14	144195	F: CAATCGGCTCTTTCCAGTTTGGC R: CAAGGACCAGAGATTCGTGAGC	143
SLC2A4	solute carrier family 2 member 4	6517	F: CCATCCTGATGACTGTGGCTCT R: GCCACGATGAACCAAGGAATGG	133
SLC7A11	solute carrier family 7 member 11	23657	F: TCCTGCTTTGGCTCCATGAACG R: AGAGGAGTGTGCTTGCGGACAT	122
SPC24	SPC24, NDC80 kinetochore complex component	147841	F: GGGATTATGAGTGTGAGCCAGG R: ACTCCAGAGGTAGTCGCTGATG	122
TIA1	TIA1 cytotoxic granule associated RNA binding protein	7072	F: GCCTAATGGTTGGCAAGTTCCTG R: CCATTTTGCCCTTGAGGCGGTT	135
TIGAR	TP53 induced glycolysis regulatory phosphatase	57103	F: CCAAAGCAGCCAGGGAAGAGTG R: CCGCTTCTTTCAGGATTAGTTGAC	123
UPF1	UPF1, RNA helicase and ATPase	5976	F: AACGAGCACCAAGGCATTGGCT R: GGCTGCTTTGATAGTGCCTTCG	116
ZBTB18	zinc finger and BTB domain containing 18	10472	F: CTGTCAAGTCCAGCCTTTCAGG R: CACTCTCATCACAGGAAGCCTC	123

Table S4 ChIP Primers

Name	Sequence	Product size(bp)
P53RRA -#1	F: GTGTGTTGCCGGAGTCGCCTTCTAT	151
	R: GTCAAGAATCCTGGGGAACCCGCTC	
P53RRA -#2	F: AGCGGGTTCCCCAGGATTCTTGA	141
	R: CAGCCTCGCATTCGCCTCAAAGACC	
GPR162-#1	F: ATCACCTTCTACCAGACACTGTGGG	145
	R: CCTCCACCACAATGGCTGGTACCTC	
GPR162-#2	F: GAGGTACCAGCCATTGTGGTGGAGG	104
	R: CTGACCAAGTTGGTGACCTGCAGGG	
ZBTB18-#1	F: CAGGAGTGTAGAGGAGTAGCATATG	133
	R: CTCCCTGTCTGTGTGTTAGAAT	
ZBTB18-#2	F: TCCACTTTGCATCTGTCTCTCTTAG	133
	R: AATCTAATCTCTTGCTACTCCTACC	
SLC1A5-#1	F: GATGCAAGCTGTCCAGGGTATTAAG	132
	R: TGGCGTGCTAGCCCTGAGGCATTGT	
SLC1A5-#2	F: ACAATGCCTCAGGGCTAGCACGCCA	120
	R: CAGCCCCTACTCATGCCTCAGCCCG	
SLC2A4-#1	F: CAAACTCTAAACCCCAGGCGGAGGG	123
	R: GACGCGAGAAGCCCCCGCCACCTCG	
SLC2A4-#2	F: GCTTGTGGCTGTGGGTCCCATCGGG	131
	R: CAGGGGCGGCGAAGATGAAAGAACC	
SLC2A14-#1	F: CAACCTGACTTTTGTTCACAATGCA	131
	R: CTGACTCTTCTCCAGAGTGGAGGTC	
SLC2A14-#2	F: CCGGACAACCCCGACCGCGAGCCGG	114
	R: GTCCGTTAATGTGGTTACAAAACGT	
SLC7A11-#1	F: AGTTGGTGTGACAGGCAGGCGCTTA	122
	R: TCTCAATTCTCCACCTCCTCGTTCC	
SLC7A11-#2	F: GGAACGAGGAGGTGGAGAATTGAGA	123
	R: CTCAGCGCTATAGTGTTCACAGGTG	

Table S5 Identified lncRNA expression in cancer compared to normal tissues

Changes	Symbol
Up	LOC650226; LOC440354; LOC400752; LOC285758; LOC100506801; LOC100288778; LOC100132287; LINC00869; LOC595101; LOC100507373; LOC100506023; LOC100272228; LOC100271836
Down	LINC00472; LOC595101; LOC399753; LOC100630923; LOC728554; LOC653501; LOC440354; LOC100630923; LOC100505989; LOC100132287; LINC00641; LINC00482; LINC00439; LINC00273; LINC00173; LINC00339; LINC00115; LINC00086

Table S6 RNA-IP identified P53RRA binding Proteins

Protein Names	Descriptions
BCAS2	Pre-mRNA-splicing factor
CIRBP	Cold-inducible RNA-binding protein
DDX1	ATP-dependent RNA helicase DDX1
DDX39A	ATP-dependent RNA helicase DDX39A
DDX39B	Spliceosome RNA helicase DDX39B
DDX3X	ATP-dependent RNA helicase DDX3X
DDX3Y	ATP-dependent RNA helicase DDX3Y
DHX29	ATP-dependent RNA helicase DHX29
EWSR1	RNA-binding protein EWS
FUS	RNA-binding protein FUS
G3BP1	Ras GTPase-activating protein-binding protein 1
G3BP2	Ras GTPase-activating protein-binding protein 2
IGF2BP1	Insulin-like growth factor 2 mRNA-binding protein 1
IGF2BP3	Insulin-like growth factor 2 mRNA-binding protein 3
KHDRBS1	KH domain-containing, RNA-binding, signal transduction-associated protein 1
PNO1	RNA-binding protein PNO1
RBMX	RNA-binding motif protein, X chromosome
RBM25	RNA-binding protein 25
RBM27	RNA-binding protein 27
RBM39	RNA-binding protein 39
RBM47	RNA-binding protein 47
RBM4B	RNA-binding protein 4B
SERBP1	Plasminogen activator inhibitor 1 RNA-binding protein

Reference

1. Shi Y, Tao Y, Jiang Y, Xu Y, Yan B, Chen X, et al. Nuclear epidermal growth factor receptor interacts with transcriptional intermediary factor 2 to activate cyclin D1 gene expression triggered by the oncoprotein latent membrane protein 1. Carcinogenesis 2012;33(8):1468-78.
2. Jiang Y, Yan B, Lai W, Shi Y, Xiao D, Jia J, et al. Repression of Hox genes by LMP1 in nasopharyngeal carcinoma and modulation of glycolytic pathway genes by HoxC8. Oncogene 2015;34(50):6079-91.
3. Dixon SJ, Stockwell BR. The role of iron and reactive oxygen species in cell death. Nat Chem Biol 2014;10(1):9-17.
4. Dixon SJ, Lemberg KM, Lamprecht MR, Skouta R, Zaitsev EM, Gleason CE, et al. Ferroptosis: an iron-dependent form of nonapoptotic cell death. Cell 2012;149(5):1060-72.

Supplementary Figures and Figure Legends

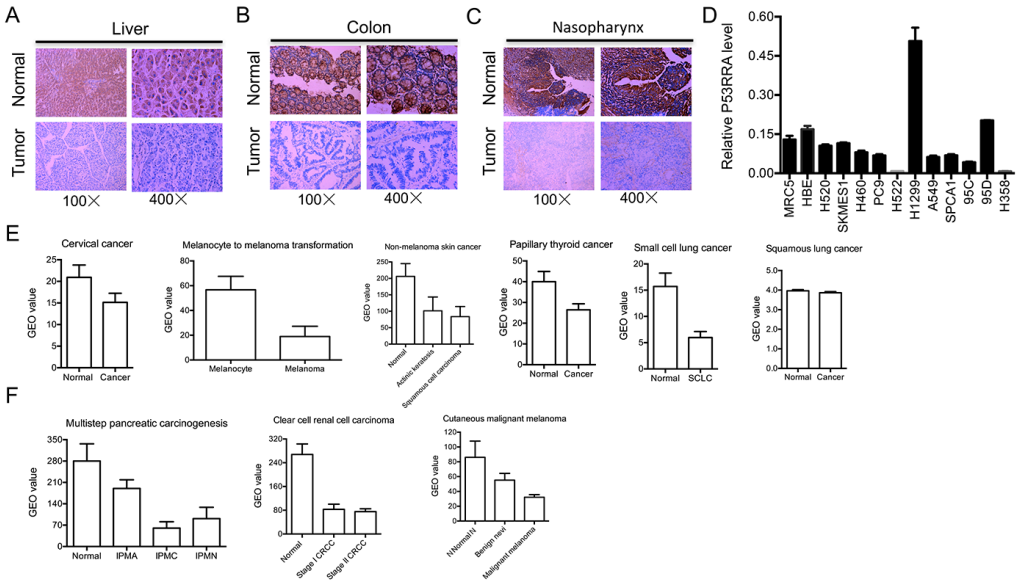

Figure S1. P53RRA RNA levels are downregulated in cancer tissues and cells.

(A-C) ISH analysis of P53RRA is shown in different cancer tissues. *In situ* hybridization was used to analyze the level of P53RRA in liver (A), colon (B) and nasopharyngeal cancers (C). (D) Real time RT-PCR analyses detecting the mRNA level of P53RRA in a panel of lung cancer cells. (E-F) GEO analysis of P53RRA in several cancers.

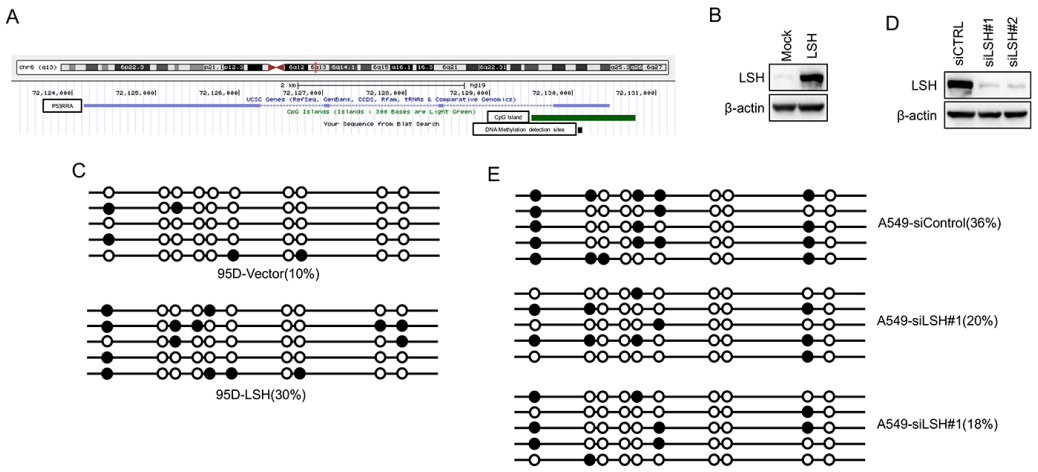

Figure S2. LSH increases DNA methylation in the promoter of P53RRA.

(A) Schematic model of bisulfite sequencing primer sites. (B) Western Blot analysis of the LSH protein level in 95D cells after their overexpression of LSH. (C) Genomic DNA derived from LSH-overexpressing 95D cells was examined by bisulfite sequencing at the promoter region of P53RRA. (D) Western Blot analysis of LSH protein expression of LSH in A549 cells after the stable knockdown of LSH. (E) Genomic DNA derived from A549 cells after the depletion of LSH was examined by bisulfite sequencing at the promoter region of P53RRA.

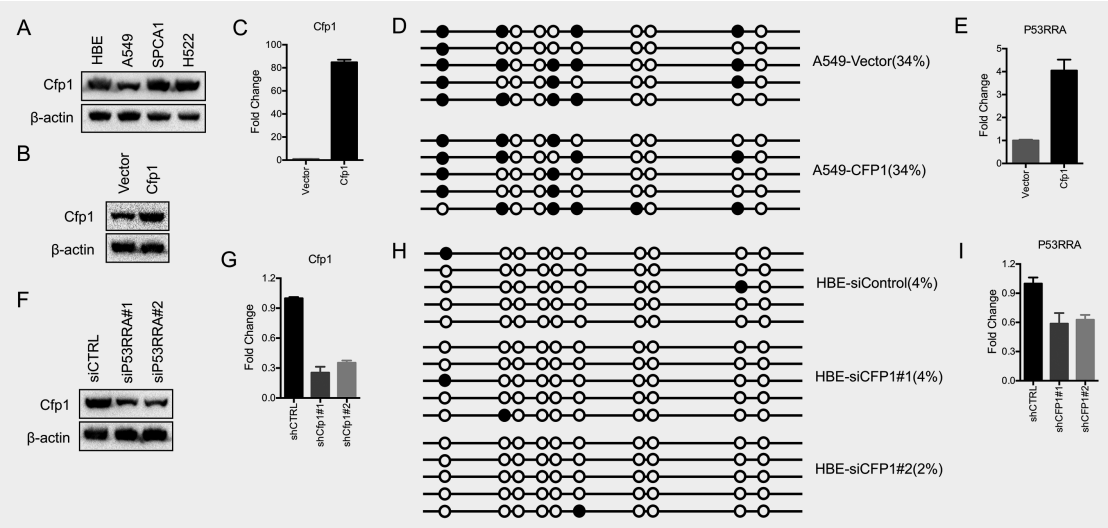

Figure S3. Cfp1 does not affect DNA methylation of P53RRA.

(A) Western blotting was used to analyze Cfp1 protein levels in a panel of lung cancer cells. (B-C) Western blotting (B) and qRT-PCR (C) were used to analyze the Cfp1 expression level in A549 cells that was highly expressed Cfp1. (D) Genomic DNA derived from A549 cells that was highly expressed Cfp1 was examined by bisulfite sequencing at the P53RRA promoter region. (E) P53RRA level derived from A549 cells that was highly expressed Cfp1 were examined by qRT-PCR. (F-G) Western blotting (F) and qRT-PCR (G) were used to analyze the Cfp1 expression in SPCA-1 cells with Cfp1 knocked down. (H) Genomic DNA derived from SPCA-1 cells with Cfp1 depleted was examined by bisulfite sequencing at the promoter region of P53RRA. (I) P53RRA level derived from SPCA-1 cells with Cfp1 depleted were examined by qRT-PCR.

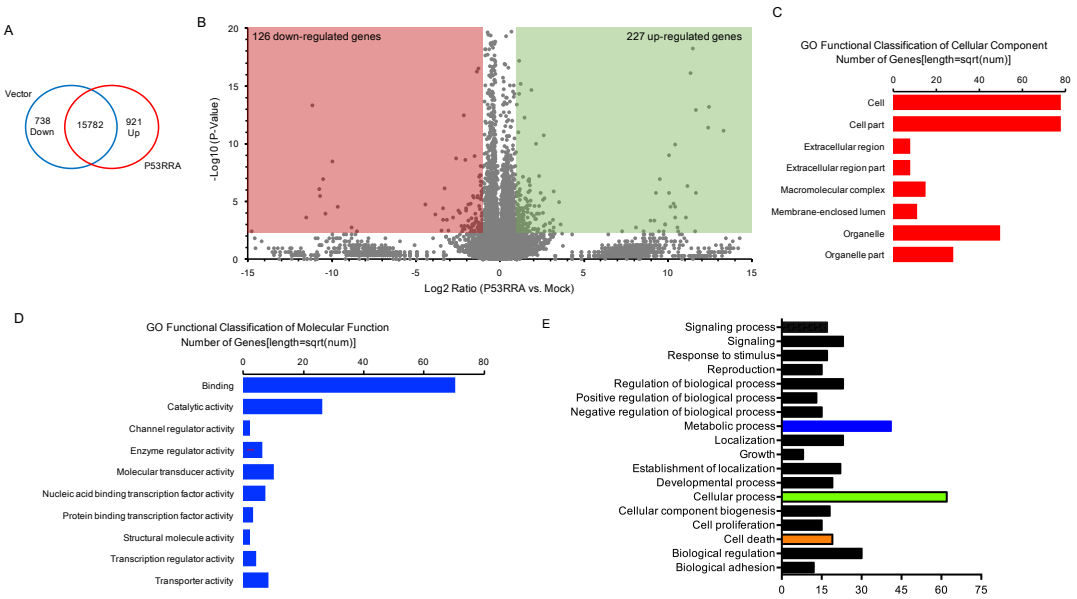

Figure S4. Analysis of RNA sequencing.

(A) P53RRA overexpression induced the downregulation 1,661 genes and the upregulation of 1,286 genes in H522 cells. (B) Volcano plot showing two vertical lines, which are the 2-fold change boundaries, and a horizontal line, which is the statistical significance boundary. (C, D) GO functional classification of cellular components (C) and molecular function (D). (E) The P53RRA-positively correlated genes in H522 cells were significantly involved in the regulation of cellular processes and metabolic processes according to their gene ontology from DAVID.

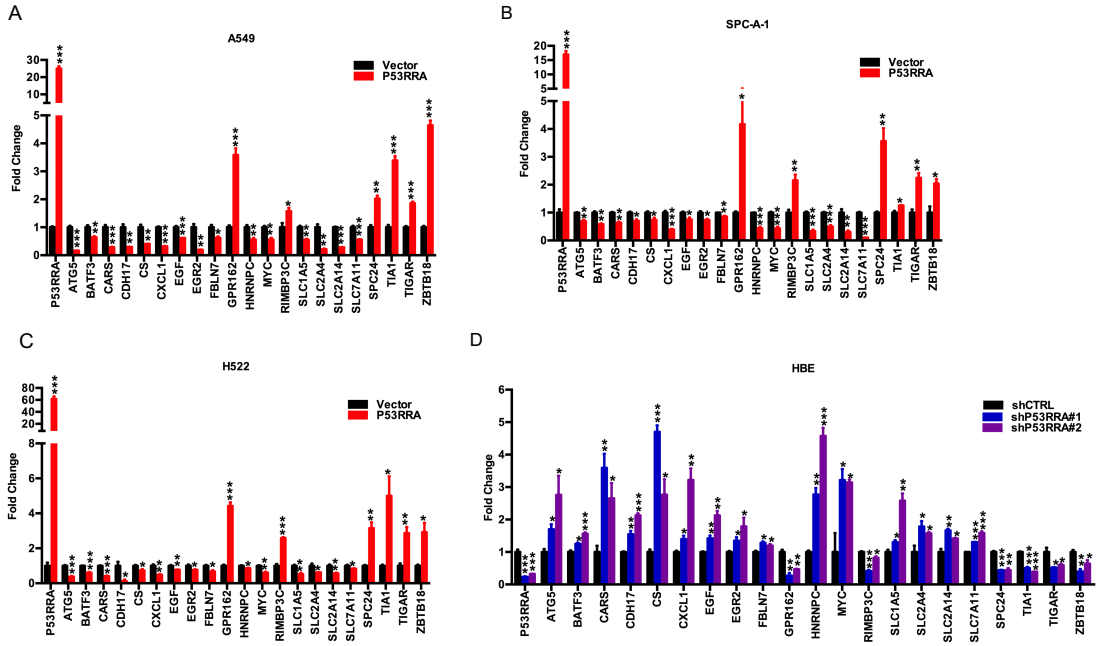

Figure S5. P53RRA affects the expression level of metabolic genes at the transcriptome level.

(A-C) The mRNA expression of the indicated genes was measured by qPCR in A549 (A), SPCA1 (B) and H522 (C) cells that overexpressing P53RRA. (D) The mRNA expression of the indicated genes was measured by qPCR after the depletion of P53RRA in HBE cells. * P<0.05, ** P<0.01, *** P<0.001.

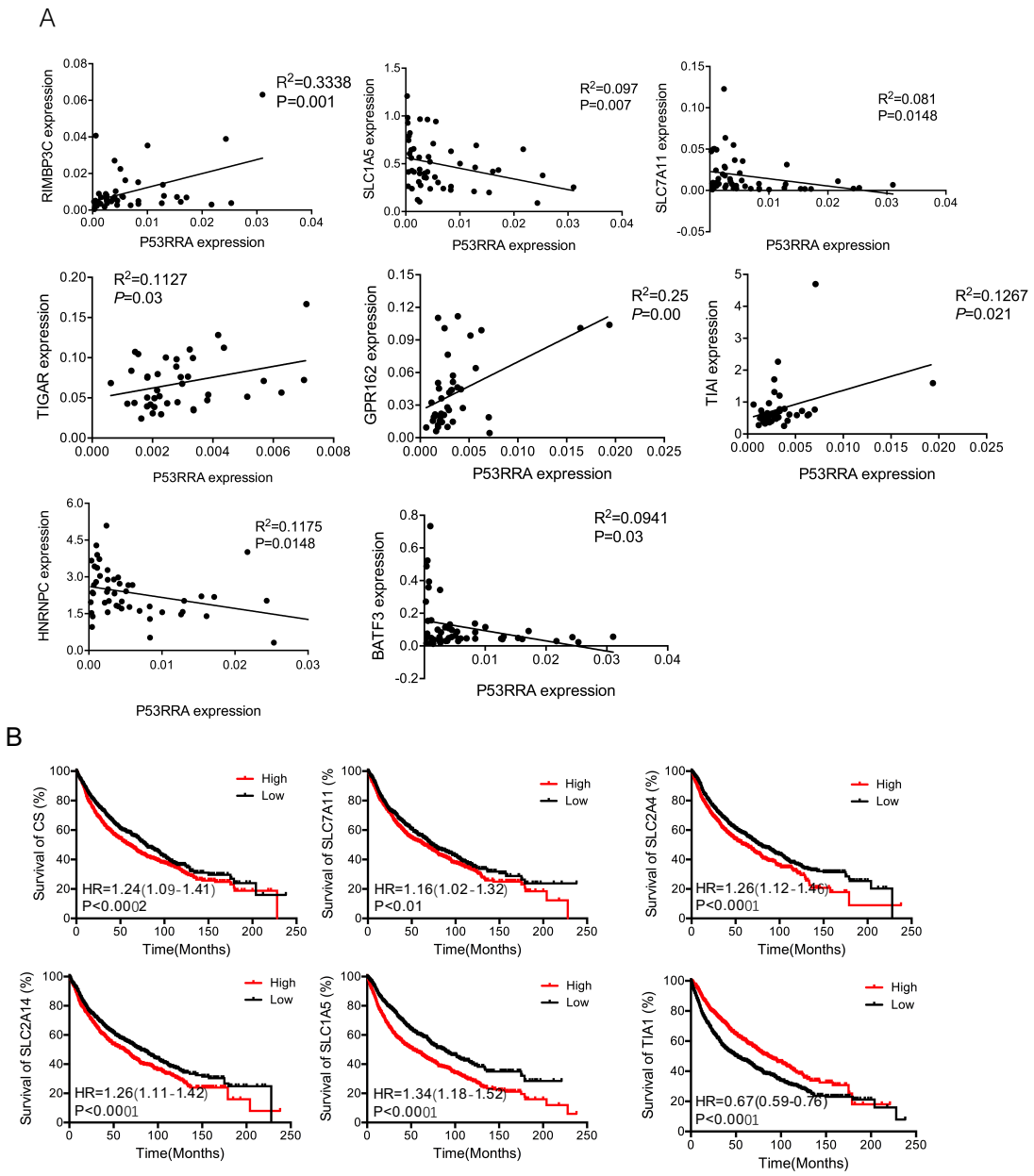

Figure S6. P53RRA affects the expression level of metabolic genes.

(A) The correlation between P53RRA levels and the mRNA levels of RIMBP3, UPF1, SLC1A5, SLC7A11, TIGAR, GPR162, TIAI, HNRNPC and BATF3 in normal lung tissues adjacent to tumors (*n*=67). The RNA levels were determined by qRT-PCR relative to GAPDH. The R values and P values are from Pearson's correlation analysis. (B) Kaplan-Meier curves for overall survival rates based on lung cancer samples expressing the indicated genes.

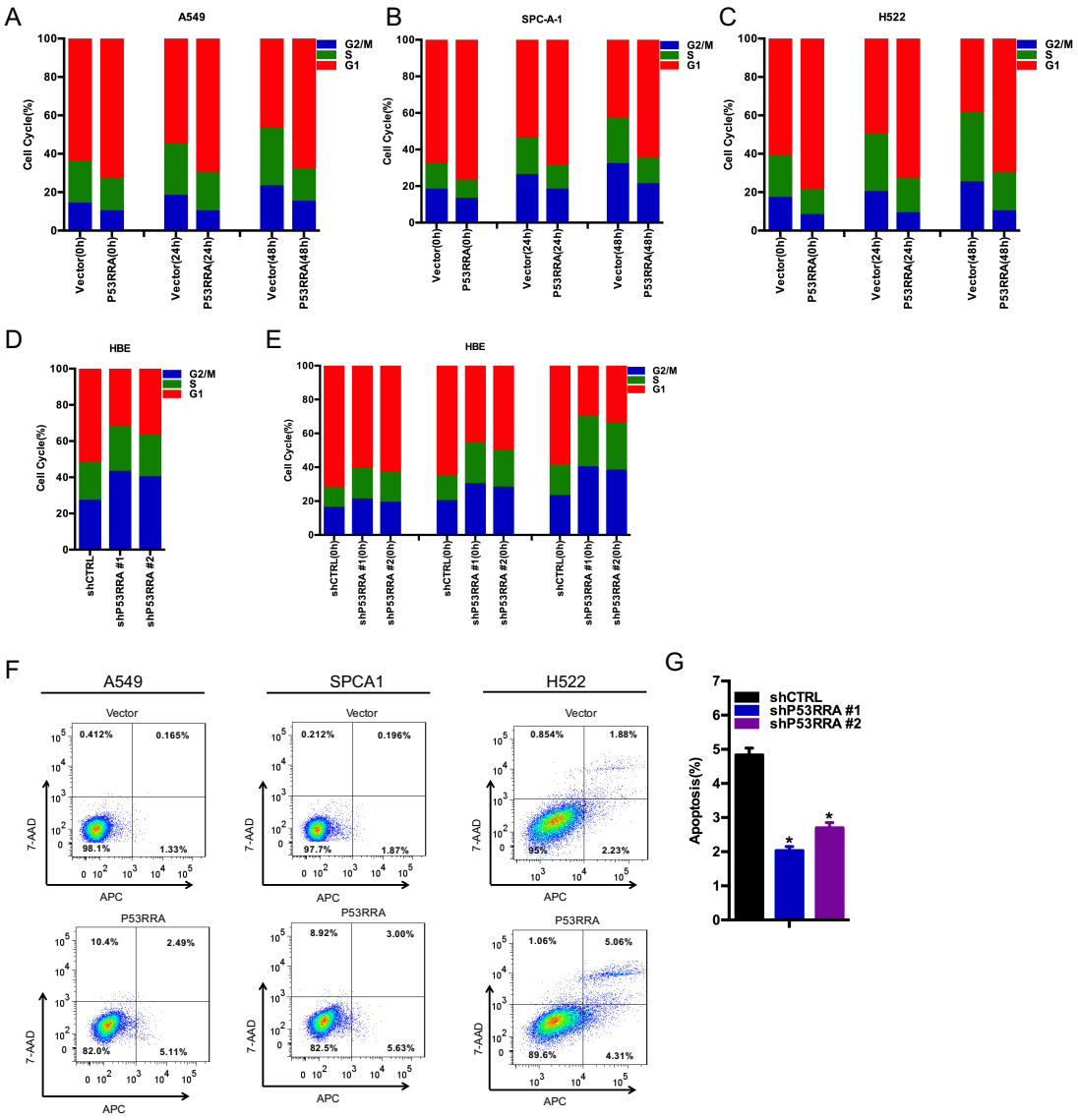

Figure S7. P53RRA promotes cell cycle progression and apoptosis.

(A-C) The effect of P53RRA on cell cycle progression in synchronized A549(A), SPCA1(B) and H522 (C) cells stably overexpressing P53RRA was analyzed using FACS. (D-E) The effect of depletion of P53RRA in synchronized HBE cells on the cell cycle progression (D) was analyzed using FACS (E). (F) FACS showed that P53RRA promoted apoptosis in A549, SPCA1 and H522 cells after stable overexpression of P53RRA. (G) Depletion of P53RRA in HBE cells attenuated apoptosis. * $P<0.05$, ** $P<0.01$.

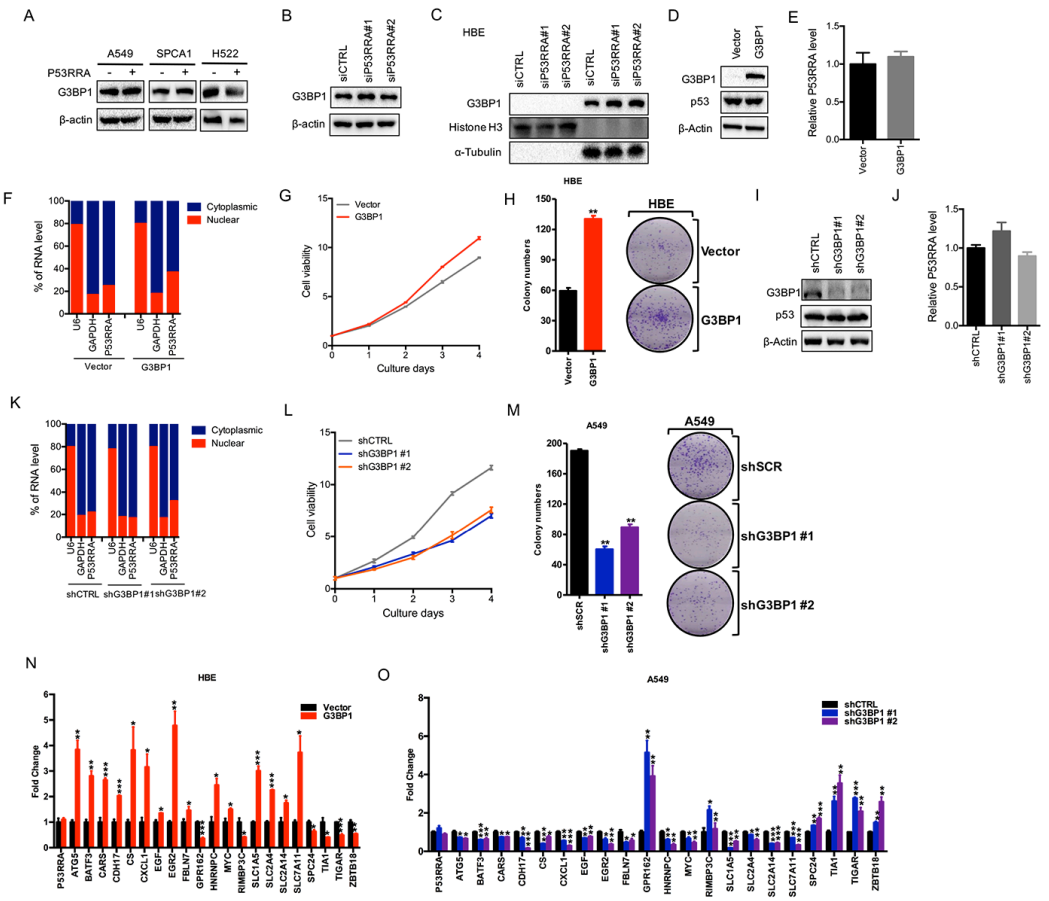

Figure S8. G3BP1 does not affect the expression and sublocalization of P53RRA but promotes lung cancer progression.

(A) P53RRA did not affect G3BP1 protein level in A549, SPCA1 and H522 cells overexpressing P53RRA. (B) The expression of G3BP1 in P53RRA-depleted HBE cells was detected by Western blot analysis. (C) The nuclear and cytoplasmic extracts from P53RRA-depleted HBE cells show that G3BP1 was located in the cytoplasm, and that the depletion of P53RRA did not change this sublocalization. (D) Western Blot showing overexpression of G3BP1 in HBE cells. (E) The overexpression of G3BP1 in HBE cells did not change the P53RRA expression levels according to RT-PCR. (F) The overexpression of G3BP1 in A549 cells did not change the P53RRA expression level according to RT-PCR. (G) MTT assays were used to assess cell viability in HBE cells that were stably transfected with G3BP1. (H) Plate

colony formation assay was measured in HBE cells that were stably transfected with G3BP1. (I) Western blot showing depletion of G3BP1 in A549 cells. (J) The depletion of G3BP1 in A549 cells did not change P53RRA expression. (K) The depletion of G3BP1 in A549 cells did not change P53RRA expression in the cytoplasm. (L) MTT assays were used to assess cell viability in A549 cells that were stably depletion of G3BP1. (M) Plate colony formation assay was measured in HBE cells after depletion of G3BP1. (N) The mRNA expression of the indicated genes was evaluated by qPCR in G3BP1-overexpressing HBE cells. (O) The mRNA expression of genes measured by qPCR in A549 cells depleted of G3BP1. * $P<0.05$, ** $P<0.01$, *** $P<0.001$.

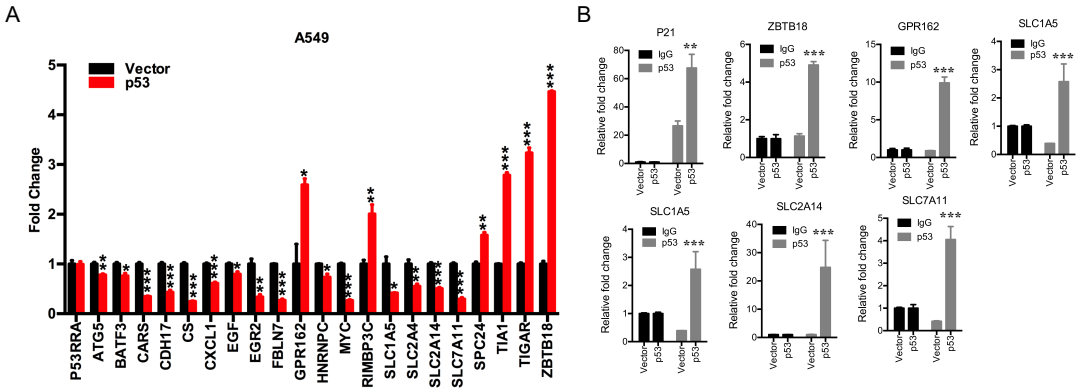

Figure S9. p53 regulates P53RRA target genes.

(A) The mRNA expression of the indicated genes as measured by qPCR in A549 cells that p53 was highly expressed. (B) ChIP assays indicated that p53 is recruited to the promoters of metabolic genes in A549 lung cancer cells that p53 was highly expressed. * P<0.05, ** P<0.01, *** P<0.001.

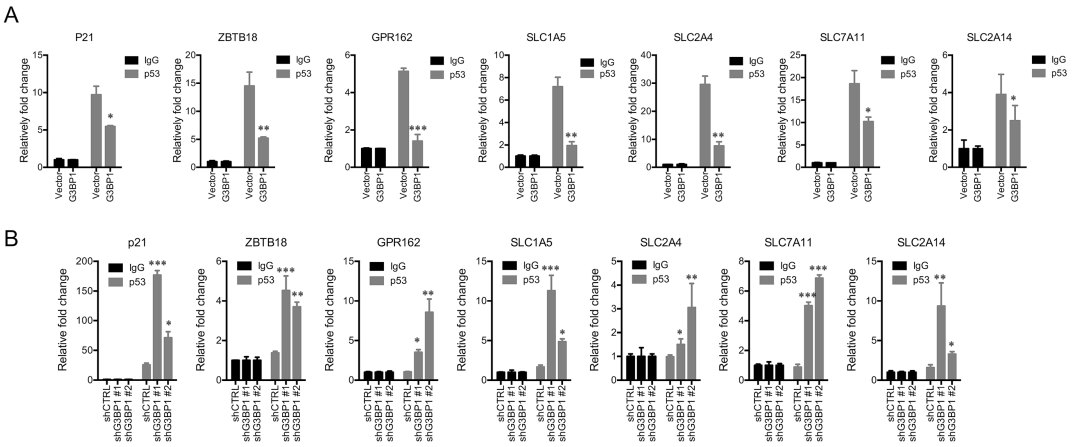

Figure S10. G3BP1 regulates the recruitment of p53 to P53RRA target gene.

(A) ChIP assays indicated that p53 is recruited to the promoters of metabolic genes in A549 lung cancer cells that overexpress G3BP1. (B) ChIP assays indicated that p53 is recruited to the promoters of metabolic genes in A549 lung cancer cells depleted of G3BP1. * P<0.05, ** P<0.01, *** P<0.001.

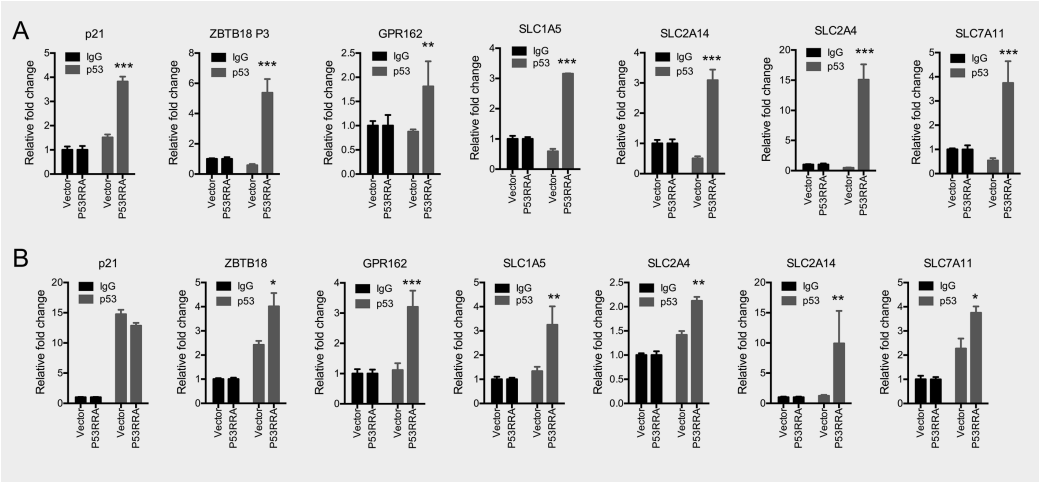

Figure S11. P53RRA regulates the recruitment of p53 to P53RRA target genes. (A-B) ChIP assays indicated that p53 was recruited to the promoters of metabolic genes in P53RRA-overexpressing H522 (A) and SPCA1 (B) lung cancer cells. * P<0.05, ** P<0.01, *** P<0.001.

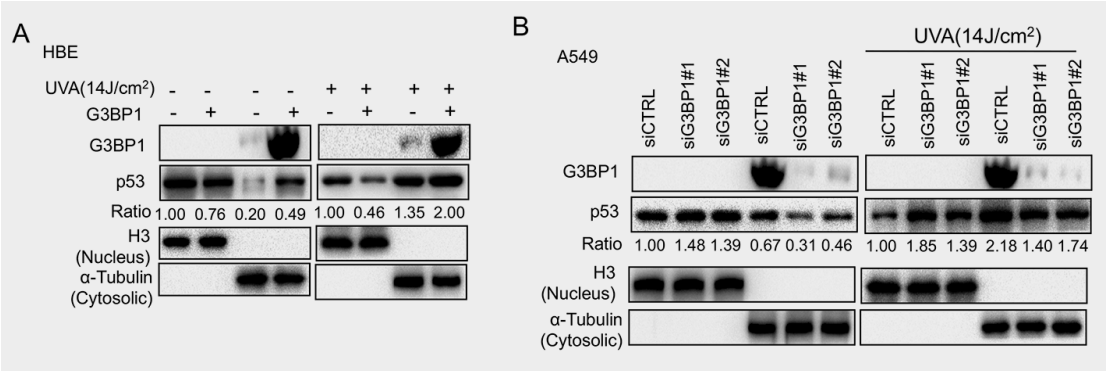

Figure S12. G3BP1 promotes the cytoplasmic distribution of p53.

(A) Nuclear and cytoplasmic extracts from A549 cells overexpressing G3BP1 showed that G3BP1 sequestered less p53 in the cytoplasm, whereas UVA treatment induced greater accumulation of p53 in the cytoplasm. (B) The nuclear and cytoplasmic extracts from HBE cells in the depletion G3BP1 showed that G3BP1 sequestered less p53 in the cytoplasm, whereas UVA treatment induced greater accumulation of p53 in the cytoplasm.

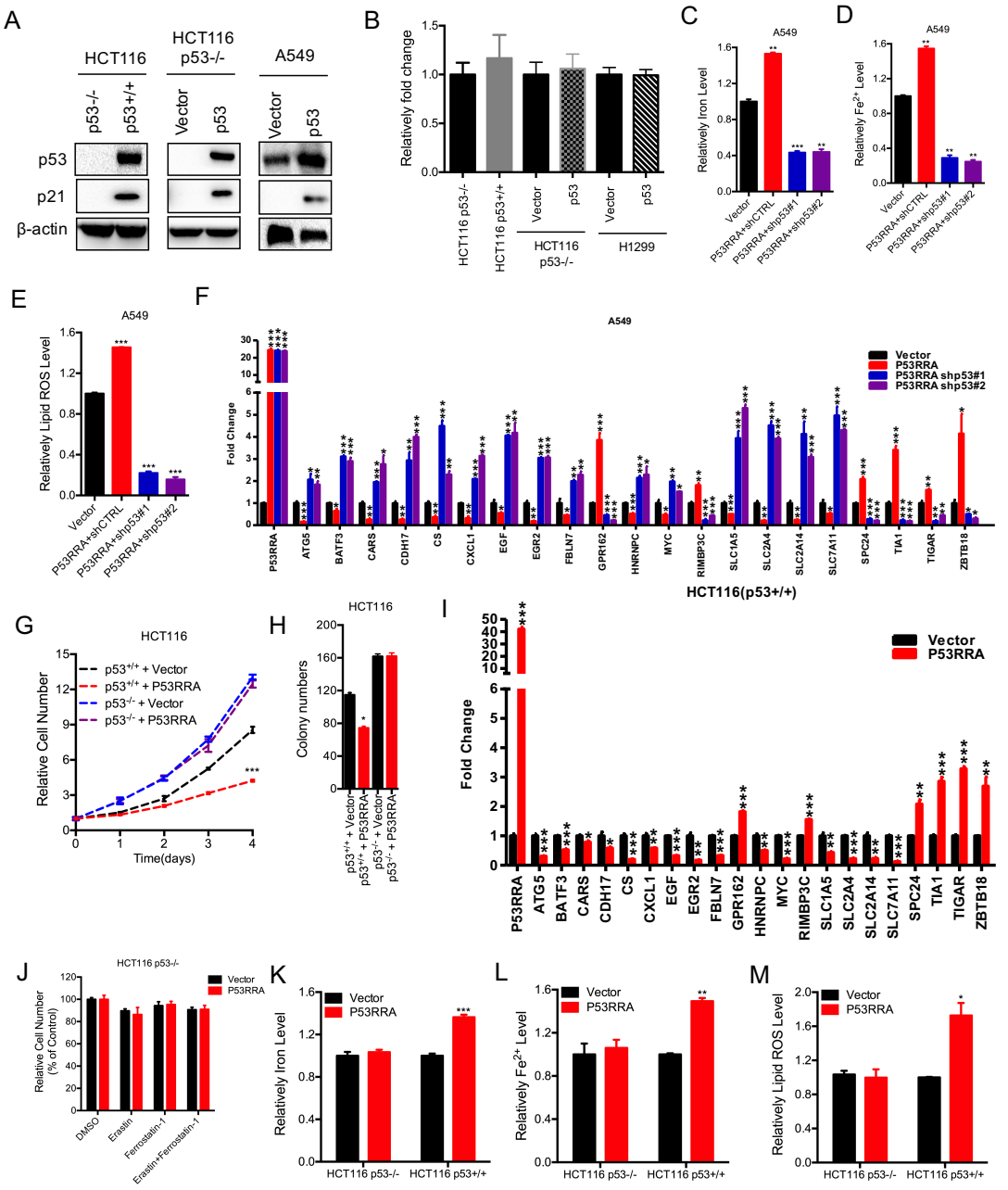

Figure S13. p53 does not affect P53RRA expression and P53RRA regulates p53 signaling pathway in a p53-dependent manner.

(A) Western blot showing p53 expression in the indicated cells. (B) The relative expression of P53RRA in different cells after the introduction of p53. (C-D) The levels of total iron (C) and ferrous iron (D) levels were analyzed in overexpression of P53RRA in A549 cells following depletion of p53. (E) The level of lipid ROS in overexpression of P53RRA in A549 cells following depletion of p53

were measured by C11-BODIPY staining coupled with flow cytometry. (F) The RNA expression of the indicated genes was measured by qPCR overexpression of P53RRA in A549 cells following depletion of p53. (G) MTT assays were used to analyze in HCT116 $p53^{+/+}$ and HCT116 $p53^{-/-}$ cells that were stably transfected with P53RRA. (H) Plate colony formation assay was measured in HCT116 $p53^{+/+}$ and HCT116 $p53^{-/-}$ cells that were stably transfected with P53RRA. (I) The RNA expression of the indicated genes was measured in HCT116 $p53^{+/+}$ cells that were stably transfected with P53RRA. (J) MTT assays were used to analyze the reponse of HCT116 $p53^{-/-}$ cells stably transfected with P53RRA to erastin (5 μM) ± Ferrostatin (1 μM). (K-L) The levels of total iron (K) and ferrous iron (L) were analyzed in HCT116 $p53^{+/+}$ and HCT116 $p53^{-/-}$ cells that were stably transfected with P53RRA. (M) The levels of lipid ROS were analyzed in HBE cells after depletion of P53RRA. * $P<0.05$, ** $P<0.01$, *** $P<0.001$.

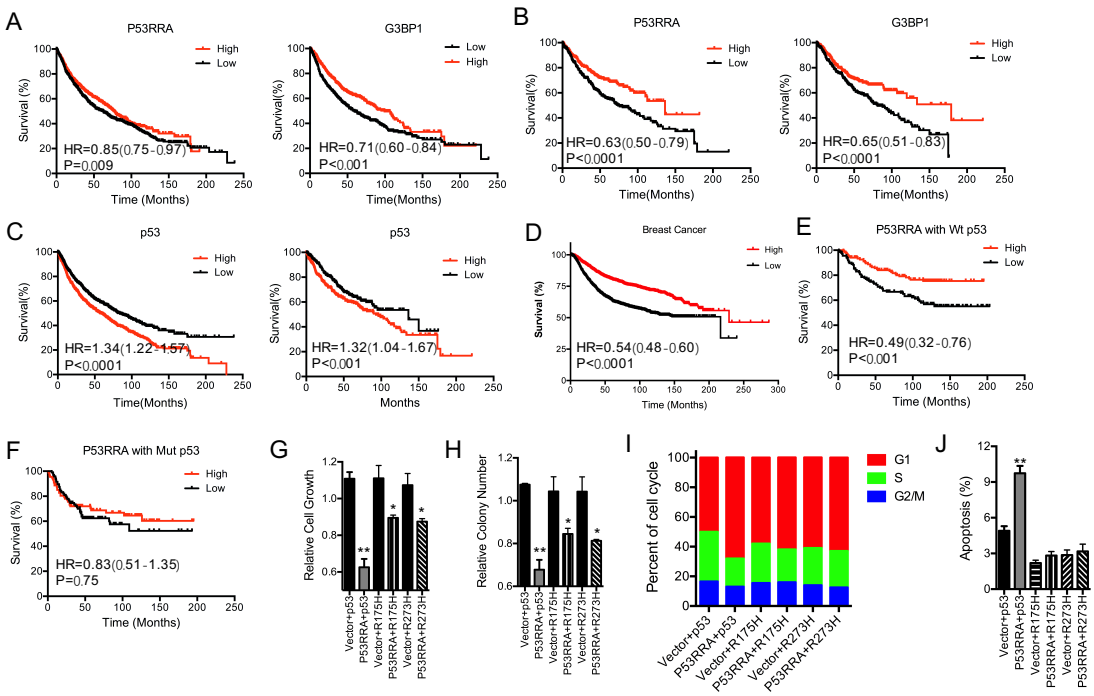

Figure S14. P53RRA reduction predicts poor clinical outcome in patients with cancer**.** (A-B) Lung cancer tissue-associated P53RRA and G3BP1 expression levels are significantly reduced. The Kaplan-Meier curves for overall survival rates associated with the measured samples are plotted here for lung cancer (A) and lung ADCs (B). (C) The lung cancer tissue-associated p53 levels are significantly elevated in lung cancer (left) and ADCs (right). (D) Breast cancer tissue-associated P53RRA expression levels are significantly reduced. (E) The cancer tissue-associated P53RRA in cancers containing wild-type p53 is significantly elevated. (F) The cancer tissue-associated P53RRA in cancers containing wild-type p53 is slightly elevated. (G) Cell growth was analyzed in relation to P53RRA and wild-type p53 or mutant p53 in HCT116 p53-/- cells. (H) Colony numbers were analyzed in relation to P53RRA and wild-type p53 or mutant p53 HCT116 p53-/- cells. (I-J) Effects of P53RRA on the cell cycle progression (I) and apoptosis (J) in HCT116 p53-/- cells in relation to P53RRA and wild-type p53 or mutant p53. * P<0.05, ** P<0.01, *** P<0.001.

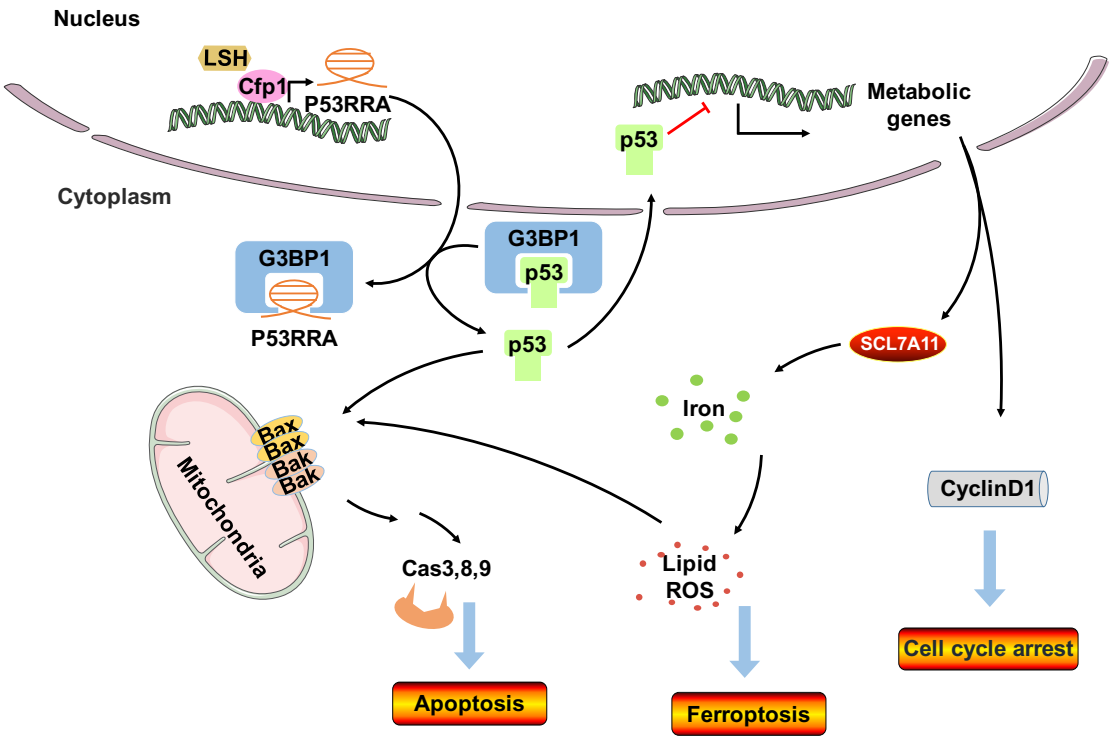

Figure S15. A schematic model of the function of the lncRNA P53RRA as a tumor suppressor in cancer progression.

The chromatin modifier LSH silences P53RRA directly, while Cfp1 activates P53RRA expression. The increase in P53RRA enhances its interaction with G3BP1 in the cytoplasm. Moreover, the p53-interacting region of G3BP1 includes the same motif as the P53RRA-interacting domain of G3BP1. P53RRA sequesters more p53 into the nucleus after P53RRA binds to the G3BP1 RRM binding motif. In turn, p53 is sequestered in the nucleus after the release of the G3BP1-p53 complex. P53RRA regulates metabolic genes, including SLC7A11 and TIGAR, which promotes the accumulation of lipid ROS and intracellular iron, promoting ferroptosis as well as apoptosis and cell cycle arrest in a p53-dependent manner.